DOI: https://doi.org/10.53256/COSE_250103

MODELING OF LOCAL SCOUR AROUND CIRCULAR STRUCTURES USING THE OPEN-SOURCE CFD TOOLBOX REEF3D

Tina Ebrahimi[a,*], Widar. W. Wang[a], Hans Bihs[a]
[a]*Norwegian University of Science and Technology, Høgskoleringen 7A, 7491 Trondheim, Norway*

[*]*Corresponding author: tina.ebrahimi@ntnu.no (Tina Ebrahimi)*

ABSTRACT: The presence of a structure in the marine environment can significantly alter the surrounding flow field. When the flow encounters a structure, such as a bridge pier, a complex three-dimensional velocity field develops. In front of the pier, a downward-directed flow forms due to stagnation pressure, generating a horseshoe vortex as the vertical flow interacts with the seabed. In addition, a vortex street develops in the wake region behind the pier. This complex flow field governs both the depth and spatial pattern of the resulting scour hole. A comprehensive three-dimensional numerical model implemented in the open-source CFD toolbox REEF3D is employed to simulate local scour around marine structures under steady current conditions. The approach is based on the solution of the Reynolds-averaged Navier–Stokes (RANS) equations, closed with the k–ω turbulence model, and coupled with a sediment transport model. In this study, dynamic free-surface evolution is captured using an interface-capturing level-set method. Furthermore, to enhance numerical stability and accurately represent the structure geometry, a direct-forcing immersed boundary method is applied. The objective of the study is to evaluate how accurately the numerical simulations reproduce both the temporal evolution and the final geometry of the scour hole observed in laboratory experiments. The time-dependent development of the scour pattern under an oscillatory free surface is simulated. A comparison between numerical results and experimental measurements is performed to assess model accuracy. The results indicate that the simulated maximum scour depth agrees with the experimental value within a few percent, and the overall scour morphology is reproduced with good fidelity. These findings demonstrate that the proposed modelling framework provides a robust basis for investigating complex scour processes and can be extended to more challenging hydraulic conditions.

KEYWORDS: Local scour, Free surface, Level set method, Direct forcing method, CFD, REEF3D.

1 INTRODUCTION

Marine structures can significantly alter local flow patterns, generating complex three-dimensional flow fields that increase turbulence intensity and bed shear stress (Graf and Istiarto, 2002). These flow modifications typically induce local scour around the structure, potentially compromising structural stability. The scour pattern develops progressively over time, expanding both in depth and lateral extent. A thorough understanding of scour formation under various hydrodynamic conditions is therefore essential to mitigate these hazards (Fredsøe and Sumer, 2002).

One of the most common examples of local scour occurs around bridge piers. As the flow approaches the pier, a complex three-dimensional velocity field develops. A downward-directed flow forms at the upstream face of the pier due to stagnation pressure, generating a horseshoe vortex, while a vortex street forms downstream in the wake region (Bihs, 2011). These flow structures strongly influence both the geometry and maximum depth of the resulting scour hole.

Olsen and Melaaen (1993) developed the first three-dimensional numerical model of local scour, simulating the initial stages under steady flow conditions using a finite-volume formulation and the k–ε turbulence model. Olsen and Kjellesvig (1998) extended this work to model the complete temporal development of scour under transient flow conditions, validating their results against empirical formulations. Roulund et al. (2005) conducted combined numerical and experimental investigations of flow and scour around bridge piers under steady currents using the k–ω turbulence model.

Baykal et al. (2015, 2017) investigated flow and local scour around vertical cylinders under combined wave–current conditions; however, free-surface effects were not explicitly resolved. To incorporate free-surface dynamics, Liu and García (2008) applied the Volume-of-Fluid (VOF) method to simulate scour around a vertical pile. Bihs and Olsen (2008) performed numerical simulations of pier scour and reported good agreement between numerical predictions and experimental data. Subsequently, Bihs (2011) examined the effect of bed slope on the initiation of sediment motion. In a later study, Bihs and Olsen (2011) demonstrated that accounting for reduced bed shear stress on sloping beds improved numerical predictions of abutment scour under steady current conditions.

Afzal et al. (2015) and Ahmad et al. (2015) employed the numerical code REEF3D to simulate scour around a large-diameter pier. Their results under both wave and steady current conditions showed that scour depth and sediment deposition increase with increasing Keulegan–Carpenter number. Ahmad et al. (2018) further investigated scour around side-by-side piles, incorporating free-surface capturing to analyse wave-induced scour. They examined the influence of key parameters, including the Keulegan–Carpenter number and pile spacing, on scour development. Gautam et al. (2021) presented a fully three-dimensional CFD model in REEF3D to simulate combined wave–current-induced scour using a level-set method for free-surface tracking. Fleit et al. (2023) applied REEF3D::CFD to simulate scour around submerged bridge decks, combining the level-set method with a ghost-cell immersed boundary method.

All previous scour studies conducted with REEF3D relied on the ghost-cell immersed boundary approach. More recently, a direct-forcing immersed boundary method has been implemented in REEF3D (Larkermani et al., 2025; Soydan et al., 2024a, 2025) for flow applications, enhancing numerical stability and interface representation.

The objective of the present study is to employ a three-dimensional numerical model within the open-source CFD toolbox REEF3D (Bihs et al., 2016) to simulate complex free-surface flow patterns and local scour around marine structures under steady current conditions. The novelty of this work lies in the first implementation of the direct-forcing immersed boundary method combined with dynamic free-surface capturing for sediment transport modelling in REEF3D. The evolving free surface is resolved using a level-set approach to accurately capture the fluid–air interface. Furthermore, the density interpolation scheme used within the direct-forcing method reduces non-physical spurious velocities at the fluid–structure interface.

The numerical model is validated through detailed comparison with experimental measurements to assess its predictive capability.

2 NUMERICAL MODEL

2.1 *REEF3D::CFD*

Computational Fluid Dynamics (CFD) modelling provides a powerful framework for the numerical simulation of scour processes. In this study, the numerical framework REEF3D::CFD developed by Bihs et al. (2016) is employed to model the local scour process. The hydrodynamic model is based on the three-dimensional, incompressible Reynolds-averaged Navier–Stokes (RANS)

equations, which represent the conservation of mass and momentum:

$$\frac{\partial u_i}{\partial x_i} = 0 \quad (1)$$

$$\frac{\partial u_i}{\partial t} + u_j \frac{\partial u_i}{\partial x_j} = -\frac{1}{\rho}\frac{\partial p}{\partial x_i} + \frac{\partial}{\partial x_j}\left[(\nu + \nu_t)\left(\frac{\partial u_i}{\partial x_j} + \frac{\partial u_j}{\partial x_i}\right)\right] + g_i \quad (2)$$

where u_i denotes the velocity components, $\rho$the fluid density, p the pressure, ν the kinematic viscosity, ν_t the eddy viscosity, and $g_i$the gravitational acceleration. The inclusion of eddy viscosity in the diffusion term reflects the application of the Boussinesq eddy-viscosity approximation to represent turbulence effects.
The k–ω turbulence model (Wilcox, 1994) is used to compute the eddy viscosity ν_t by solving two additional transport equations for the turbulent kinetic energy k and the specific dissipation rate ω:

$$\frac{\partial \mathrm{k}}{\partial \mathrm{t}} + \mathrm{u_j}\frac{\partial \mathrm{k}}{\partial \mathrm{x_j}} = \frac{\partial}{\partial \mathrm{x_j}}\left[\left(\nu + \frac{\nu_\mathrm{t}}{\sigma_\mathrm{k}}\right)\frac{\partial \mathrm{k}}{\partial \mathrm{x_j}}\right] + \mathrm{P_k} - \beta_\mathrm{k}\mathrm{k} \quad (3)$$

$$\frac{\partial \omega}{\partial t} + u_j\frac{\partial \omega}{\partial x_i} = \frac{\partial}{\partial x_j}\left[\left(\nu + \frac{\nu_t}{\sigma_\omega}\right)\frac{\partial \omega}{\partial x_j}\right] + \frac{\omega}{k}\alpha P_k - \beta\omega^2 \quad (4)$$

where the turbulent production term P_k is defined as:

$$P_k = \nu_t \frac{\partial u_i}{\partial x_j}\left[\frac{\partial u_i}{\partial x_j} + \frac{\partial u_j}{\partial x_i}\right] \quad (5)$$

and the model constant coefficients are as follows:

$$\alpha = \frac{5}{9},\ \beta = \frac{3}{40},\ \beta_k = \frac{9}{100},\ \sigma_\omega = \sigma_k = 2 \quad (6)$$

A signed distance function, referred to as the level-set function, is used to represent the air–water interface. The solid boundaries and mobile bed are also represented using the level-set method. The continuous signed-distance function $\phi(\mathbf{x}, t)$ defines the minimum distance to the interface Γ. For the free surface, the level-set function is defined as:

$$\phi(\vec{x}, t) = \begin{cases} > 0, & \text{if } \vec{x} \in \text{phase 1} \\ = 0, & \text{if } \vec{x} \in \Gamma \\ < 0, & \text{if } \vec{x} \in \text{phase 2} \end{cases} \quad (7)$$

The evolution of the interface is governed by the convection equation:

$$\frac{\partial \phi}{\partial t} + u_j\frac{\partial \phi}{\partial x_j} = 0 \quad (8)$$

To maintain the signed-distance property, the level-set function is reinitialised after each time step following (Sussman et al., 1994):

$$\frac{\partial \phi}{\partial \mathrm{t}} + \mathrm{sign}(\phi)\left(\left|\frac{\partial \phi}{\partial \mathrm{x_j}}\right| - 1\right) = 0 \quad (9)$$

where $\mathrm{sign}(\phi)$ denotes the smoothed sign function (Peng et al., 1999). For mass conservation, the Eikonal condition $|\ \partial\phi/\partial x_j\ | = 1$must be satisfied. The density and viscosity fields are defined as:

$$\rho = \rho_\omega H(\phi) + \rho_a\left(1 - H(\phi)\right) \quad (10)$$

$$\nu = \nu_\omega \mathrm{H}(\phi) + \nu_\mathrm{a}\left(1 - \mathrm{H}(\phi)\right) \quad (11)$$

where subscripts w and a denote water and air properties, respectively. To smooth sharp interface gradients, a regularised Heaviside function $H(\phi)$ is employed with an interface thickness$\epsilon = 2.1\ \Delta\mathrm{x}$:

$$H(\phi) = \begin{cases} 0, & \text{if } \phi < -\epsilon \\ \frac{1}{2}\left(1 + \frac{\phi}{\epsilon} + \frac{1}{\pi}\sin\left(\frac{\pi\phi}{\epsilon}\right)\right), & \text{if } |\phi| \le \epsilon \\ 1, & \text{if } \phi > \epsilon \end{cases} \quad (12)$$

A staggered rectilinear grid is employed together with high-order spatial and temporal discretisation schemes. In the staggered grid arrangement, density and viscosity are directly evaluated at cell faces, reducing unphysical oscillations associated with interpolation procedures (Bihs et al., 2016; Larkermani et al., 2024).
Convective terms in the RANS equations are discretised using a fifth-order Weighted Essentially Non-Oscillatory (WENO) scheme (Jiang and Shu, 1996). The Hamilton–Jacobi formulation of the WENO scheme is applied to the level-set equation as well as to the transport equations for turbulent kinetic energy and specific dissipation rate (Jiang and Peng, 2000). The WENO approach provides high accuracy while enhancing numerical stability.
Temporal integration is performed using a Total Variation Diminishing (TVD) Runge–Kutta scheme. A third-order TVD Runge–Kutta method is applied to the level-set convection equation, while a second-order TVD Runge–Kutta scheme is used for the momentum equations (Shu and Osher, 1988). Diffusion terms are treated implicitly, removing the diffusion restriction from the CFL stability condition (Bihs et al., 2016).
The pressure field is computed using the projection method (Chorin, 1968). The resulting Poisson equation is solved using the BiCGSTAB iterative solver (Van der Vorst, 1992) from the HYPRE high-performance preconditioner library, employing the semi-coarsening multigrid preconditioner PFMG (Ashby and Falgout, 1996).

2.2 *Morphological model*

Sediment transport is initiated when the bed shear stress exceeds the critical bed shear stress (τ_c). The bed shear stress can be related to the turbulent kinetic energy near the bed under the assumption that turbulence production and dissipation are in equilibrium:

$$\tau_b = \sqrt{C_\mu}\rho k \tag{15}$$

where the constant C_μ has a value of 0.09. An accurate determination of the critical bed shear stress is essential for reliable scour prediction. The critical bed shear stress is calculated as:

$$\tau_c = \theta_c(\rho_s - \rho)gd \tag{16}$$

where θ_c is the critical shields parameter, ρ_s is the sediment density, ρ is the water density, and d is the particle diameter. The classical Shields diagram (Shields, 1936) is applicable primarily to beds with small gradients under fully submerged conditions. However, steeper bed slopes promote sediment motion due to the downslope component of gravitational force (Zanke et al., 2023). As the bed slope increases, the critical bed shear stress decreases, thereby enhancing erosion. In this study, the modified critical bed shear stress proposed by Fredsøe and Deigaard (1992), which accounts for both longitudinal and transverse bed slopes through a reduction factor, is adopted.
The bedload transport rate is calculated using the formulation of Engelund and Fredsøe (1976) as:

$$q_b = \sqrt{\frac{(\rho_s-\rho)g}{\rho}}\, d \begin{cases} 0, & \text{if } \theta < \theta_c \\ 18.74(\theta - \theta_c)(\theta^{0.5} - 0.7\theta_c^{0.5}), & \text{if } \theta > \theta_c \end{cases} \tag{17}$$

where θ is the shields parameter, defined as:

$$\theta = \frac{\tau_b}{(\rho_s-\rho)gd} \tag{18}$$

The mobile bed is represented by the zero level set of the level-set function, eliminating the need for remeshing. Bed-level variations and morphological evolution are computed using the Exner equation, which ensures sediment mass conservation within each computational cell (Paola and Voller, 2005):

$$\frac{\partial z_b}{\partial t} + \frac{1}{(1-n)}\left[\frac{\partial q_{b,x}}{\partial x} + \frac{\partial q_{b,y}}{\partial y}\right] = 0 \tag{19}$$

where, z_b is the bed level, $q_{b,x}$ is the bed load transport in x-direction, $q_{b,y}$ is the bed load transport in y-direction, and n is the porosity of the bed sediment.

The bed slope may approach the angle of repose, particularly for non-cohesive sediments. When this threshold is exceeded, a sand-slide mechanism occurs, representing slope failure. In such cases, excess sediment collapses downslope, and the bed angle is reduced, typically by approximately 2° (Roulund et al., 2005). The present morphological model incorporates a sand-slide mechanism to prevent numerical instability, limit excessive reductions in bed shear stress, and provide a more realistic representation of sediment redistribution (Burkow and Griebel, 2016). Both slope-induced reduction of critical shear stress and the sand-slide mechanism are essential for accurate prediction of local scour (Bihs and Olsen, 2008). In contrast to the rapid evolution of the hydrodynamic field, morphological changes occur over much longer time scales. To reduce computational cost, a decoupled approach is adopted: the morphological model is updated using a larger time step than the hydrodynamic solver. Numerical stability is ensured by adaptively limiting the time step according to the Courant–Friedrichs–Lewy (CFL) condition (Griebel et al., 1998).

3 NUMERICAL SETUP

A pier-scour case based on the experimental study of Link (2006) under clear-water steady current conditions was used to evaluate the capability of the direct-forcing-based sediment transport module implemented in REEF3D::CFD. The experiments were conducted in the hydraulic laboratory of the Technical University of Darmstadt in a flume 37 m long, 2 m wide, and 1 m deep. Several tests were performed with varying flow velocities and water depths. The flume sidewalls were constructed of Plexiglas.
A cylindrical Plexiglas pile with a diameter of 0.2 m was installed 16 m downstream of the flume inlet. Sediment layers 1.5 m in length were placed both upstream and downstream of the pier, while the remaining sections of the flume consisted of a concrete bed. Aluminium plates sealed the interface between the sediment bed and the concrete floor to prevent horizontal seepage through the sediment layer. The scour geometry was measured using a laser distance sensor mounted inside the pier; consequently, bed topography outside the immediate scour hole was not recorded.
Natural sand was used as bed material, with a median grain diameter $d_{50} = 0.97$mm, sediment density $\rho_s = 2650$ kg/m^3, and an angle of repose of 29°. The selected experimental case corresponds to a flow velocity of 0.3 m/s, a still-

water depth of 0.3 m, and a total experimental duration of 21 hours.

The numerical domain represents a three-dimensional channel 4.5 m long, 2 m wide, and 0.8 m deep, with a water depth of 0.3 m. A cylindrical pier with a diameter of 0.2 m is positioned 1.5 m downstream of the inlet boundary. The bed consists of a 0.3 m thick sediment layer. The critical Shields parameter for incipient motion is set to $\theta_c = 0.035$.

At the inlet, a logarithmic velocity profile corresponding to a depth-averaged velocity of 0.3 m/s (equivalent to a discharge of 0.18 m³/s) is prescribed. A zero-gradient condition is applied to pressure at the inflow boundary. Wall functions are used for the velocity field, and the k–ω turbulence model employs rough-wall functions for the turbulence quantities $k$and ω. The sidewalls are treated as no-slip boundaries. At the outlet, a zero-gradient condition is imposed for velocity, while pressure is prescribed using a Dirichlet condition consistent with the fixed water level.

Figure 1 illustrates the initial configuration of the numerical flume. The initial condition consists of still water with a depth of 0.3 m and a flat sediment bed with uniform material properties. REEF3D's initialization procedure is applied for velocity, pressure, and turbulence variables. A potential-flow solution is used to initialize the velocity field, while a hydrostatic distribution is applied for pressure. The turbulence quantities k and ω are initialized according to the applied wall-function formulation.

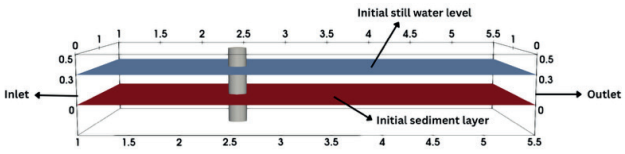

Figure 1. Numerical flume configuration used in the REEF3D simulations.

4 NUMERICAL RESULTS

The bed-load transport rate is calculated using the formulation proposed by Engelund and Fredsøe (1976). Bed shear stress is estimated using a turbulent kinetic energy-based formulation, incorporating an appropriate reduction coefficient to improve the prediction of sediment transport. As the primary focus of this study is the dominant mechanism of scour under clear-water steady-current conditions, suspended sediment transport is neglected.

The prescribed depth-averaged flow velocity is 0.3 m/s, corresponding to a discharge of 0.18 m³/s. The hydrodynamic module of REEF3D has been extensively validated in previous studies (e.g., Kamath et al., 2019; Ahmad et al., 2019). Therefore, the present study concentrates primarily on evaluating the performance of the morphological model.

4.1 *Convergence study*

A grid convergence study was performed to determine the minimum spatial resolution required for accurate simulation of the scour process. The Courant–Friedrichs–Lewy (CFL) number was fixed at 0.3 to ensure numerical stability of both the hydrodynamic and morphological models. Model performance was evaluated by comparing the time evolution of the maximum scour depth with the experimental data reported by Link (2006).

Four uniform grid resolutions were tested: $\Delta x = \Delta y = \Delta z = 0.05$ m, 0.03 m, 0.01 m, and 0.0075 m, while maintaining a constant CFL number of 0.3. Figure 2 presents the numerical results for the temporal development of the maximum scour depth around the circular pier under steady-current conditions for the four grid sizes.

The comparison indicates that coarser meshes produce significant deviations from the experimental measurements. Refining the mesh from 0.05 m to 0.03 m and subsequently to 0.01 m leads to progressively improved predictions of scour depth evolution and better agreement with the experimental data. A satisfactory match is obtained with the 0.01 m grid resolution. Further refinement to 0.0075 m increases computational cost substantially, while only marginal improvement in accuracy is observed. Therefore, a grid resolution of 0.01 m is considered sufficient for simulating local scour around a cylindrical pier under steady-current conditions.

To provide a quantitative assessment, the root-mean-square error (RMSE) between the experimental and numerical maximum scour depths was computed as:

$$\mathrm{RMSE} = \sqrt{\frac{1}{n}\sum_{i=1}^{n}(y_i - \hat{y}_i)^2} \qquad (20)$$

where y_i represents the experimental values from Link (2006) and $\hat{y}_i$ denotes the corresponding numerical predictions. As shown in Figure 3, the RMSE decreases consistently with mesh refinement from 0.05 m to 0.01 m. The results confirm that the 0.01 m grid resolution provides an optimal balance between computational efficiency and predictive accuracy. For this grid, the corresponding y^+ value is approximately 175, which lies within the recommended range of 30–300 for wall-function-based turbulence modelling.

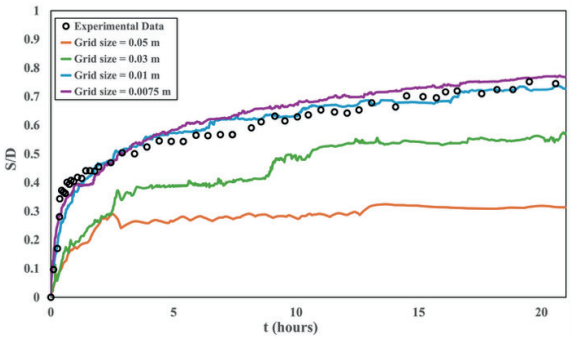

Figure 2. Convergence study showing the time evolution of the maximum scour depth around a vertical pier under steady-current conditions, compared with experimental data from Link (2006).

4.2 *Pier scour under steady current conditions*

In this section, the scour results obtained using the selected grid resolution of 0.01 m are presented in detail. The simulation required approximately 4.5 hours of wall-clock time to reproduce 21 hours of physical scour development, using 512 processors in parallel.

Figure 4 shows that, for an approaching flow velocity of 0.3 m/s, the velocity increases to approximately 0.43 m/s on both sides of the pile. This acceleration is caused by flow contraction due to the obstruction created by the pier. In contrast, the horizontal velocity decreases to approximately −0.14 m/s in the wake region downstream of the pier, primarily due to the shielding effect of the structure. Flow separation and the formation of wake vortices are clearly visible in Figure 4.

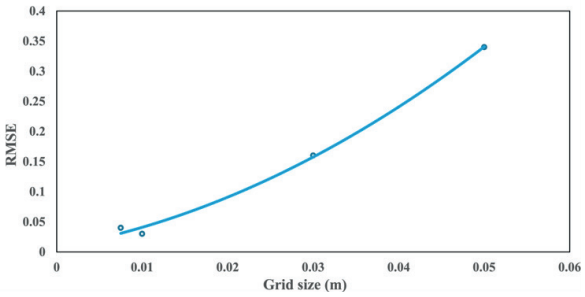

Figure 3. Root-mean-square error (RMSE) between numerical and experimental maximum scour depth for different grid resolutions.

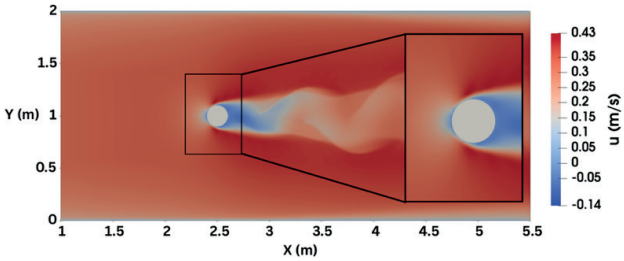

Figure 4. Contours of simulated horizontal velocity, u (m/s), around the pile at $T = 21\,h$.

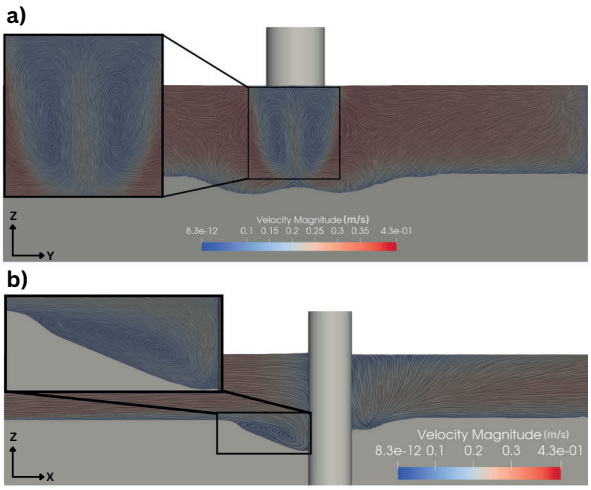

Figure 5. (a) Formation of counter-rotating vortices downstream of the pile; (b) horseshoe vortex upstream of the pile and velocity magnitude around the cylinder (m/s).

Figure 5a illustrates the formation of counter-rotating vortices downstream of the pier, which enhance near-bed turbulence, while Figure 5b shows the horseshoe vortex upstream of the pier generated by the adverse pressure gradient at the bed. These results demonstrate that the numerical model is capable of accurately capturing the complex three-dimensional flow structure and separation phenomena around the pier.

Consistent with the experimental observations, the simulated temporal evolution of scour indicates that the initial maximum scour depth develops at the sides of the pier and subsequently migrates toward the upstream face. Figure 6 presents the measured scour depth contours reported by Link (2006) after 21 hours of testing. The maximum scour depth is located at the upstream face of the pier and measures 0.153 m. The corresponding simulated bed elevation from REEF3D at T = 21 h is shown in Figure 7. The predicted maximum scour depth reaches 0.145 m, which is in close agreement with the experimental value.

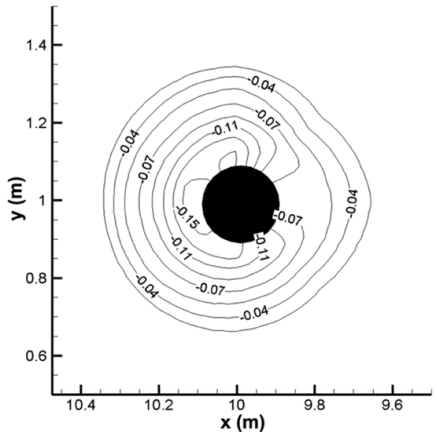

Figure 6. Experimental bed elevation contours at $T = 21$ h, with flow from left to right, as in Bihs (2011).

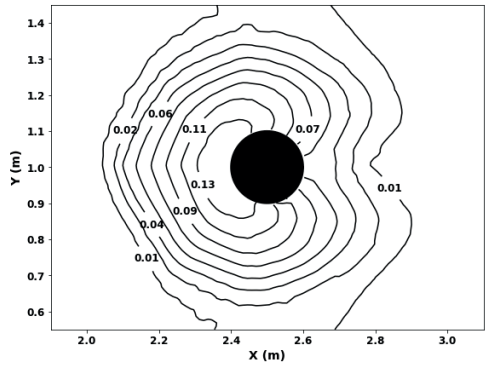

Figure 7. Numerical bed elevation contours at T = 21 h.

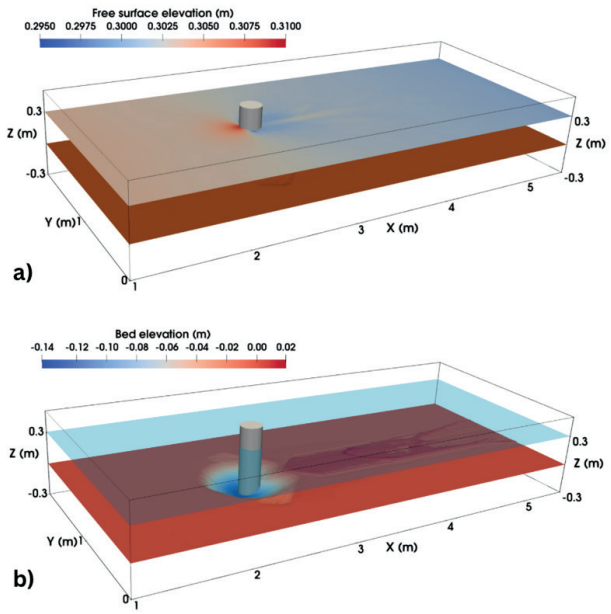

Figure 8. Three-dimensional simulated scour under steady-current conditions at $T = 21$ h: (a) free-surface elevation and (b) bed elevation.

The dynamically captured free surface, computed using the level set method, is presented together with the bed topography in Figure 8. The figure illustrates the fully three-dimensional numerical results at the end of the simulation ($T = 21\ h$).

5 CONCLUSIONS

In this study, a three-dimensional sediment transport module implemented in REEF3D was used to simulate local scour around a cylindrical pier under steady-current conditions using a direct-forcing immersed boundary approach. A mesh convergence study was conducted to determine the optimal grid resolution. The results indicate that a grid size of 0.01 m provides an appropriate balance between numerical accuracy and computational efficiency.

The simulated scour pattern and the temporal evolution of the maximum scour depth were validated against experimental measurements. The comparison demonstrates that the numerical model is capable of accurately reproducing the complex hydrodynamic processes and associated morphological changes in the vicinity of hydraulic structures.

Furthermore, the results confirm that the use of a decoupled hydrodynamic–morphological approach is an effective strategy for reducing the substantial computational cost associated with fully coupled three-dimensional scour simulations.

ACKNOWLEDGEMENTS

The authors acknowledge funding from the European Union (ERC, PARTRES, Grant No. 101045646). The views and opinions expressed are solely those of the authors and do not necessarily reflect those of the European Union or the European Research Council Executive Agency. Neither the European Union nor the granting authority can be held responsible for them. The simulations were performed on the supercomputer Betzy, provided by UNINETT Sigma2 – the National Infrastructure for High-Performance Computing and Data Storage in Norway.

REFERENCES

Afzal, S., Bihs, H., Kamath, A., Arntsen, Ø.A., (2015). Three-dimensional numerical modeling of pier scour under current and waves using level-set method. Journal of Offshore Mechanics and Arctic Engineering 137, 032001.

Ahmad, N., Afzal, S., Bihs, H., Arntsen, Ø.A., (2015). Three-dimensional numerical modeling of local scour around a non-slender cylinder under varying wave conditions, in: 36th IAHR world Congress.

Ahmad, N., Bihs, H., Myrhaug, D., Kamath, A., Arntsen, Ø.A., (2018). Three-dimensional numerical modelling of wave-induced scour around piles in a side-by-side arrangement. Coastal Engineering 138, 132–151.
Ashby, S.F., Falgout, R.D., (1996). A parallel multigrid preconditioned conjugate gradient algorithm for groundwater flow simulations. Nuclear science and engineering 124, 145–159.
Baykal, C., Sumer, B.M., Fuhrman, D.R., Jacobsen, N.G., Fredsøe, J., (2015). Numerical investigation of flow and scour around a vertical circular cylinder. Philosophical Transactions of the Royal Society A: Mathematical, Physical and Engineering Sciences 373, 20140104.
Baykal, C., Sumer, B.M., Fuhrman, D.R., Jacobsen, N.G., Fredsøe, J., (2017). Numerical simulation of scour and backfilling processes around a circular pile in waves. Coastal Engineering 122, 87–107.
Bihs, H., (2011). Three-dimensional numerical modeling of local scouring in open channel flow (Doctoral dissertation).
Bihs, H., Kamath, A., Chella, M.A., Aggarwal, A., Arntsen, Ø.A., (2016). A new level set numerical wave tank with improved density interpolation for complex wave hydrodynamics. Computers & Fluids 140, 191–208.
Bihs, H., Olsen, N.R.B., (2008). Three dimensional numerical modeling of pier scour, in: Fourth International Conference on Scour and Erosion, ICSE 4, Tokyo, Japan.
Bihs, H., Olsen, N.R.B., (2011). Numerical modeling of abutment scour with the focus on the incipient motion on sloping beds. Journal of Hydraulic Engineering 137, 1287–1292.
Burkow, M., Griebel, M., (2016). A full three dimensional numerical simulation of the sediment transport and the scouring at a rectangular obstacle. Computers & Fluids 125, 1–10.
Chorin, A.J., (1968). Numerical solution of the navier-stokes equations. Mathematics of computation 22, 745–762.
Engelund, F., Fredsøe, J., (1976). A sediment transport model for straight alluvial channels. Hydrology Research 7, 293–306.
Fleit, G., Baranya, S., Ehlers, R., Bihs, H., 2023. Cfd modeling of flow and local scour around submerged bridge decks. Journal of Coastal and Hydraulic Structures 3.
Fredsoe, J., Deigaard, R., (1992). Mechanics of coastal sediment transport. volume 3. World scientific publishing company.
Fredsoe, J., Sumer, B.M., (2002). The mechanics of scour in the marine environment. volume 17. World Scientific Publishing Company.
Gautam, S., Dutta, D., Bihs, H., Afzal, M.S., 2021. Three-dimensional computational fluid dynamics modelling of scour around a single pile due to combined action of the waves and current using level-set method. Coastal Engineering 170, 104002.
Graf, W., Istiarto, I., (2002). Flow pattern in the scour hole around a cylinder. Journal of Hydraulic Research 40, 13–20.
Griebel, M., Dornseifer, T., Neunhoeffer, T., (1998). Numerical simulation in fluid dynamics: a practical introduction. SIAM.
Jiang, G.S., Peng, D., (2000). Weighted eno schemes for hamilton–jacobi equations. SIAM Journal on Scientific computing 21, 2126–2143.
Jiang, G.S., Shu, C.W., (1996). Efficient implementation of weighted eno schemes. Journal of computational physics 126, 202–228.
Kamath, A., Fleit, G., Bihs, H., 2019. Investigation of free surface turbulence damping in rans simulations for complex free surface flows. Water 11, 456.
Larkermani, E., Bihs, H., Winckelmans, G., Duponcheel, M., Martin, T., Mu¨ller, B., Georges, L., (2024). Development of an accurate central finite-difference scheme with a compact stencil for the simulation of unsteady incompressible flows on staggered orthogonal grids. Computer Methods in Applied Mechanics and Engineering 428, 117117.
Larkermani, E., Bihs, H., Winckelmans, G., Mu¨ller, B., Georges, L., (2025). High-fidelity explicit large eddy simulations of airflows inside buildings using the immersed boundary method and orthogonal grids. Physics of Fluids 37.
Link, O., (2006). Untersuchung der kolkung an einem schlanken zylindrischen pheiler in sandigem boden. PhD thesis. Institut fr Wasserbau und Wasserwirtschaft, Technische Universitt Darmstadt.
Liu, X., Garc´ıa, M.H., (2008). Three-dimensional numerical model with free water surface and mesh deformation for local sediment scour. Journal of waterway, port, coastal, and ocean engineering 134, 203–217.
Olsen, N.R., Kjellesvig, H.M., (1998). Three-dimensional numerical flow modeling for estimation of maximum local scour depth. Journal of Hydraulic Research 36, 579–590.
Olsen, N.R., Melaaen, M.C., (1993). Three-dimensional calculation of scour around cylinders. Journal of Hydraulic Engineering 119, 1048–1054.
Paola, C., Voller, V.R., (2005). A generalized exner equation for sediment mass balance. Journal of Geophysical Research: Earth Surface 110.
Peng, D., Merriman, B., Osher, S., Zhao, H., Kang, M., (1999). A pde-based fast local level set method. Journal of computational physics 155, 410–438.
Roulund, A., Sumer, B.M., Fredsøe, J., Michelsen, J., (2005). Numerical and experimental investigation of flow and scour around a circular pile. Journal of Fluid mechanics 534, 351–401.
Shields, A., (1936). Application of similarity principles and turbulence research to bed-load movement. Technical Report. Soil Conservation Service.
Shu, C.W., Osher, S., (1988). Efficient implementation of essentially non-oscillatory shock-capturing schemes. Journal of computational physics 77, 439–471.
Soydan, A., Wang, W.W., Bihs, H., (2024a). An improved direct forcing immersed boundary method with integrated mooring algorithm for floating offshore wind turbines. Journal of Offshore Mechanics and Arctic Engineering 147, 042101.
Soydan, A., Wang, W.W., Bihs, H., (2025). An improved direct forcing immersed boundary method for floating body simulations in waves. Applied Ocean Research 158, 104523.
Sussman, M., Smereka, P., Osher, S., (1994). A level set approach for computing solutions to incompressible two-phase flow. Journal of Computational physics 114, 146–159.
Van der Vorst, H.A., (1992). Bi-cgstab: A fast and smoothly converging variant of bi-cg for the solution of nonsymmetric linear systems. SIAM Journal on scientific and Statistical Computing 13, 631–644.
Wilcox, D., (1994). Turbulence modeling for cfd, dcw industries, inc., 460 p.
Zanke, U., Roland, A., Wurpts, A., (2023). The reason for the rise in critical shear stress on sloping beds. Water 15, 2976.